PCCP

Accepted Manuscript

ROYAL SOCIETY OF CHEMISTRY

www.rsc.org/pccp

Rydberg and valence state excitation dynamics: A velocity map imaging study involving the E - V state interaction in HBr

Dimitris Zaouris, Andreas Kartakoullis, Pavle Glodic and Peter C. Samartzis
Institute of Electronic Structure and Laser, Foundation for Research and Technology-Hellas, Vassilika Vouton, 71110 Heraklion, Greece.

Helgi Rafn Hróðmarsson and Ágúst Kvaran*
Science Institute, University of Iceland, Dunhagi 3, 107 Reykjavík, Iceland.

Total number of pages in manuscript: 36
Tables: 1
Figures: 6
Manuscript file: VMI-REMPI-HBr-150301.docx

Running head title, if needed: REMPI-VMI of HBr

*Correspondence should be addressed to:

Agust Kvaran
Permanent address:
Science Institute,University of Iceland,
Dunhagi 3, 107 Reykjavík,
Iceland
Phone: +354-525-4672 (A.K. office)
Phone: +354-525-4800 (main office)
Fax: +354-552-8911 (main office)
E-mail: agust@hi.is

1

Abstract

Photoexcitation dynamics of the E ($^1\Sigma^+$) (v´= 0) Rydberg state and the $V(^1\Sigma^+)$ (v´) ion-pair vibrational states of HBr are investigated by Velocity Map Imaging (VMI). H^+ photoions, produced through a number of vibrational and rotational levels of the two states were imaged and kinetic energy release (KER) and angular distributions were extracted from the data. In agreement with previous work, we found the photodissociation channels forming $H^*(n = 2)$ + $Br(^2P_{3/2})$/$Br^*(^2P_{1/2})$ to be dominant. Autoionization pathways leading to H^+ + $Br(^2P_{3/2})$/$Br^*(^2P_{1/2})$ via either $HBr^+(^2P_{3/2})$ or $HBr^+*(^2P_{1/2})$ formation were also present. Analysis of KER and angular distributions and comparison with rotationally and mass resolved Resonance Enhanced MultiPhoton Ionization (REMPI) spectra revealed excitation transition mechanisms and characteristics of states involved as well as the involvement of the $E – V$ state interactions and their v´ and $J´$ dependence.
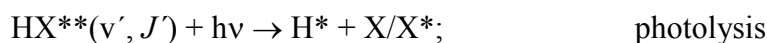
I.   INTRODUCTION

In recent years there is a growing interest and emphasis on studies of higher energy valence and Rydberg states, complementing the vast amount of information on molecular ground and low energy valence states. As the excitation energy increases, the higher density of states gives rise to more complex spectroscopy and dynamics involving state mixing, predissociation, autoionization and other interesting state interaction phenomena worth of further study.

The hydrogen halides have turned out to be ideal candidates for fundamental spectroscopy and photofragmentation studies involving higher energy valence and Rydberg states.[1-36] Since the original work by Price on the hydrogen halides (HX),[1] a wealth of spectroscopic data has been derived from absorption spectroscopy for HCl,[2,5,6,8] HBr,[3,7,9] and HI[4] and from resonance enhanced multiphoton ionization (REMPI) studies (HCl,[10-12,16,17,19-22] HBr,[13,16-19,23] and HI[14-16,24]). Extensive perturbations observed in spectra are clear indications of the importance of state interactions involved. Photofragmentation studies based on velocity map imaging (VMI) of H^+ following one-colour resonance excitations in (HCl**(v´, J´))[25-27,29,30,37] and HBr[26,27] have been performed. Recently Kvaran and coworkers have used mass resolved REMPI spectra to determine quantitative and qualitative information relevant to state interaction, photofragmentation as well as energetics of HCl,[31-33,35] HBr,[34,35] and HI.[36] The analyses are based on spectral perturbations seen as alterations or irregularities in line-shifts, line-intensities or line-widths. VMI studies and mass-resolved REMPI spectra analysis have been found to give complementary results in terms of Rydberg to ion-pair state interactions for resonance states in HCl.[29,31] Particular emphasis has been laid on studies of the strong homogenenous $(\Delta\Omega = 0)$ state interaction between the $E^1\Sigma^+$ $(\Omega = 0)$ Rydberg state and the $V^1\Sigma^+$ $(\Omega = 0)$ ion-pair state, which, together, form an adiabatic double-well potential $(B^1\Sigma^+)$ (see Fig. 1 for HBr).[25-27,30,35,37] Both
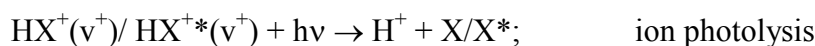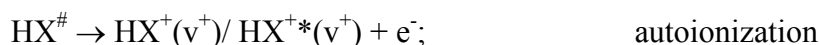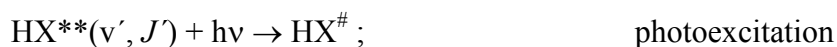
photoionization and photodissociation processes are found to be largely affected by this state mixing.

The above studies revealed the following major paths for H^+ formation of the hydrogen halides (HX) following and depending on the resonance excitation states.

i)   HX** photolysis followed by fragment ionization:

HX**(v', J') + hν → H* + X/X*;   photolysis

H* + hν → H^+ + e^-;   photoionization

ii)   HX** ionization followed by ion photolysis:

HX**(v', J') + hν → $HX^{\#}$;   photoexcitation

$HX^{\#}$ → $HX^+(v^+)$/ $HX^+*(v^+)$ + e^-;   autoionization

$HX^+(v^+)$/ $HX^+*(v^+)$ + hν → H^+ + X/X*;   ion photolysis

iii)   Ion-pair formation:

HX**(v', J') + hν → H^+ + X^- Ion-pair formation

Here X and X* (and HX^+ and HX^+*) denote the ground ($X(^2P_{3/2})$/ $HX^+(^2\Pi_{3/2})$) and spin-orbit excited ($X*(^2P_{1/2})$/ $HX^{+*}(^2\Pi_{1/2})$) species, respectively. H* is the first excited state of Hydrogen, H*(n = 2). In the case of HBr the photoexcitation steps (i) to form H* + Br and H* + Br* involve excitation to repulsive Rydberg states which converge to the repulsive molecular ion states $B^2\Sigma^+$ ($\sigma^2(\pi_x^1\pi_y^1)\sigma*^1$) and $^2\Pi$ ($\sigma^1\pi^3\sigma*^1$)[27,38] labelled, in a simplified form, as $[B^2\Sigma^+]$Ry and $[^2\Pi]$Ry (see Fig. 1), where the details inside the bracket characterize the ion core and "Ry" represents the Rydberg electron. The $[B^2\Sigma^+]$Ry state and the lower energy component of two $[^2\Pi]$Ry states correlate to the assymptotic atom pair, H* + Br, whereas the higher energy component of the

$[^2\Pi]$Ry states correlates to H* + Br* as shown in Fig. 1. Considering one-electron transitions from the mixed $E/V\ ^1\Sigma^+$ (i.e. $B\ ^1\Sigma^+$) state(s), based on the principal electron configurations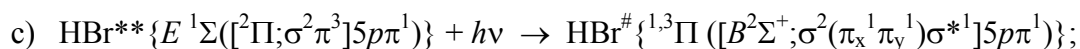 of the $E([\sigma^2\pi^3]5p\pi^1)$ and the $V(\sigma^1\pi^4\sigma^{*1})$ states, the Rydberg electron must occupy a $5p\pi$ orbital in which case, the possible Rydberg states characteristics could be $^{1,3}\Pi$ ($[B^2\Sigma^+;\ \sigma^2(\pi_x^1\pi_y^1)\sigma^{*1}]5p\pi^1$) and $^{1,3}\Sigma$ ($[^2\Pi;\sigma^1\pi^3\sigma^{*1}]5p\pi^1$) (Fig. 1). Although the selection rule for spin conservation favours the involvement of singlet Rydberg states triplet states cannot be ruled out (hence the notations $^{1,3}\Pi$ and $^{1,3}\Sigma$). Three one-electron transitions, two parallel ($\pi \to p\pi$; $\sigma \to \sigma^*$) and one-perpendicular ($\pi \to \sigma^*$) transitions, could be involved, i.e.

   a) HBr**$\{V\ ^1\Sigma(\sigma^1\pi^4\sigma^{*1})\} + h\nu \to$ HBr$^\#\{^{1,3}\Sigma\ ([^2\Pi\ ;\sigma^1\pi^3\sigma^{*1}]5p\pi^1)\}$;

                                      parallel transition

   b) HBr**$\{E\ ^1\Sigma([^2\Pi;\sigma^2\pi^3]5p\pi^1)\} + h\nu \to$ HBr$^\#\{^{1,3}\Sigma\ ([^2\Pi\ ;\sigma^1\pi^3\sigma^{*1}]5p\pi^1)\}$;

                                        parallel transition

   c) HBr**$\{E\ ^1\Sigma([^2\Pi;\sigma^2\pi^3]5p\pi^1)\} + h\nu \to$ HBr$^\#\{^{1,3}\Pi\ ([B^2\Sigma^+;\sigma^2(\pi_x^1\pi_y^1)\sigma^{*1}]5p\pi^1)\}$;
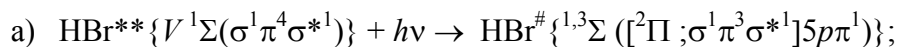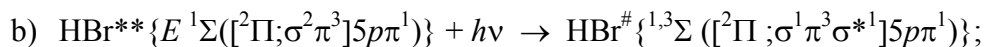
                                        perpendicular transition

-one of which (a) involves the ion-pair component (i.e. largest ion-pair /V state character) of the mixed (B) state. The weight of the ion-pair (V) character will increase (hence the Rydberg (E) character will decrease) gradually from the inner well of the mixed / B state as the internuclear distance increases to reach a maximum near the outer turning point of the outer well.

     In this paper we present the results of a VMI investigation involving the interactions between the $E^1\Sigma^+$ Rydberg state and the $V^1\Sigma^+$ ion-pair valence state in HBr. KER and angular distributions data are extracted from images of H$^+$ originating from the $E^1\Sigma^+(v'= 0; J' = 1 \text{ - } 9)$, $V^1\Sigma^+$ ($v'= m + 4;\ J'= 0 - 8$), $V^1\Sigma^+$ ($v'= m + 5;\ J'= 0 - 4$) and $V^1\Sigma^+$ ($v'= m + i, i = 6 - 10;\ J'= 0$)

states of HBr for $J' = J''$ (i.e. Q rotational lines). m is an unknown integer, since the zero

vibrational energy ($v' = 0$) is not known for the $V^1\Sigma^+$ state.[13] The contributions of paths (i) and

(ii) above were quantified, whereas channel (iii) was not detected. The relative ratio of the two

steps in (i) as well as the angular distributions are found to change with J'/v'. Trends coincide

with the E - V interaction strength measured in REMPI studies, indicating a possible connection.

II. EXPERIMENTAL

The VMI setup used in this work has been described previously[39,40] and only a brief

description will be given here. A supersonic molecular beam of HBr seeded in He is formed by a

15-30% HBr mixture in He supersonically expanding through a homemade piezoelectrically

actuated nozzle valve (1mm diameter) and being skimmed before entering the detection chamber

where the ion optics are positioned. After passing through a ~2 mm diameter hole in the repeller

electrode, the molecular beam is intersected at right angles by a laser beam focused at the

geometric focus position of a single-electrode repeller-grid arrangement. The laser beam is

generated by an Nd^{3+}:YAG pumping a master oscillator power oscillator system (Spectra Physics

MOPO).

For the VMI experiments reported here, the repeller is always ON, i.e. the apparatus is operated

in "VMI mode". The photofragments traverse a field-free time-of-flight region (45 cm) and a

gated, position-sensitive detector (dual, imaging-quality MCP array coupled to a phosphor

screen) images the photofragment sphere. The image frame is recorded asynchronously every

second (~10 laser shots) by a CCD camera and several thousand frames are averaged to form

images such as those shown in Fig. 2. The 2D slice of the 3D ion distribution from each final

image is extracted by inverse Abel transformation and integrated from its center over angle to

extract the speed and over radius to extract the angular distributions of the photofragments.

H^+ photoion images are recorded following HBr excitation to different intermediate valence and

ion-pair electronic and rovibrational levels by appropriate tuning of the laser wavelength (Table

I). Background images are recorded with the laser on and the molecular beam off and subtracted

from the signal images.

III.　　RESULTS

A. H^+ images and kinetic energy release (KER) spectra

H^+ images were recorded for two-photon resonance excitation from the ground state

$X^1\Sigma^+(v´= 0; J´´)$ to the $E^1\Sigma^+(v´= 0; J´ = 1 - 9)$ Rydberg and the $V^1\Sigma^+$ $(v´= m + 4; J´= 0 - 8)$, $V^1\Sigma^+$

$(v´= m + 5; \ J´= 0 – 4)$ and $V^1\Sigma^+$ $(v´= m + i,; i = 4 – 10; \ J´= 0)$　ion-pair states of HBr for $J´= J´´$

(i.e. Q rotational lines). The majority of the images feature two intense rings surrounded by a

number of weaker ones at higher kinetic energy release (KER) as shown in Fig. 2. Fig. 3(a)

shows the H^+ KER distributions for the E state as a function of rotational level ($J´ = 1 - 9$) of

$v´=0$, whereas Fig. 3(b) shows the V state KER distributions as a function of vibrational level

$(v´= m + i,\ i = 4 - 10)$ for $J´ = 0$. The two KER peaks around 0.1 eV and 0.5 eV, in the case of

the E ($v´=0$), state correspond to the two intense rings in each image. The weaker rings in those

images have KERs in the 1.0 - 2.2 eV region.

In order to assign each KER peak, we calculated the expected KER´s for the various

channels presented in Section I as follows:

KER("Br") $= 3h\nu + E(J´´) - D_0(HBr) - E(H^*)$

$$\text{for channel "H* + Br"; (i)} \qquad (1a)$$

$$KER(\text{"Br*"}) = 3h\nu + E(J'') - D_0(HBr) - E(H^*) - SO(Br^*)$$

$$\text{for channel "H* + Br*"; (i)} \qquad (1b)$$

$$KER(\text{"HBr}^+\text{"}) = h\nu + IE(HBr^+(3/2)) + G_0(HBr^+(3/2),v^+) - D_0(HBr) - IE(H)$$

$$\text{for channel "HBr}^+(v^+)\text{"; (ii)} \qquad (1c)$$

$$KER(\text{"HBr}^{+*}\text{"}) = h\nu + IE(HBr^+(1/2)) + G_0(HBr^+(1/2),v^+) - D_0(HBr) - IE(H) - SO(Br^*)$$

$$\text{for channel "HBr}^{+*}(v^+)\text{"; (ii)} \qquad (1d)$$

-where $h\nu$ is the photon excitation energy.[9,13,34] $D_0(HBr)$ is the bond energy for HBr (30 210 ± 40

cm^{-1} [27,41]), $E(H^*)$ is the electronic energy of H*($n = 2$) (82 258.95 cm^{-1} [27,42]) and $SO(Br^*)$ is the

spin-orbit energy of Br (3 685.24 cm^{-1} [27,42]). $IE(HBr^+(3/2))$ and $IE(HBr^{+*}(1/2))$ are the ionization

energies of HBr with respect to the formation of HBr^+ (3/2) (94 150.672 cm^{-1}) and HBr^{+*} (1/2)

(96 796.17 cm^{-1}) respectively.[43] $IE(H)$ is the ionization energy of H (109 677.61 cm^{-1} [27,42]).

$E(J'')$ is the rotational energy for the rotational level of the ground state, J'', expressed as

$$E(J'') = B''(J''(J''+1)) - D''J''^2(J''+1)^2 \qquad (2)$$

where $B'' = 8.348244$ cm^{-1} and $D'' = 3.32 \times 10^{-4}$ cm^{-1}.[19,44] $G_0(HBr^+(3/2),v^+)$ and $G_0(HBr^{+*}$

$(1/2),v^+)$ are the vibrational energies of the v^+ vibrational levels for HBr^+ (3/2) and $HBr^+ *$(1/2),

respectively, expressed as

$$G_0 = \omega_e(v^+ + 1/2) - \omega_e x_e (v^+ + 1/2)^2 + \omega_e y_e (v^+ + 1/2)^3$$

$$- (\omega_e(1/2) - \omega_e x_e (1/2)^2 + \omega_e y_e (1/2)^3) \qquad (3)$$

where $\omega_e = 2439.10$ cm^{-1}, $\omega_e x_e = 45.18$ cm^{-1}, $\omega_e y_e = 0.126$ cm^{-1} and $\omega_e = 2431.35$ cm^{-1}, $\omega_e x_e =$

44.05 cm^{-1}, $\omega_e y_e = 0.0472$ cm^{-1} for HBr^+ (3/2) and $HBr^+ *$(1/2) respectively.[43]

Based on the calculations above, the peak around 0.1 eV for the $E(v' = 0)$ state and from 0.1 to 0.7 eV (depending on v') for the V state is due to the H*$(n = 2)$ + Br*$(^2P_{1/2})$ formation followed by photoionization of H*$(n = 2)$. We will henceforth refer to this channel as the Br* channel. The peak at ~0.6 eV for the $E(v' = 0)$ state and from 0.5 eV to ~1.2 eV for the V state is assigned to the formation of H*$(n = 2)$ + Br$(^2P_{3/2})$ followed by H*$(n = 2)$ photoionization and will henceforth be referred to as the Br channel. Finally, the "multi-peak structure" ranging from 1.0 eV to 2.2 eV for the $E(v' = 0)$ state and from ~1.0 eV to 3.0 eV for the V state is due to photodissociation of several vibrational levels, v^+, of the ground HBr$^+(^2\Pi_{3/2})$ and the spin-orbit excited HBr$^{+*}(^2\Pi_{1/2})$ molecular ions, formed after photoionization of HBr**(v', J'). Those H$^+$ photofragments are produced with either a Br or a Br* co-fragment. This KER feature corresponds to pathway (ii) of Sec. I and will henceforth be referred to, collectively, as the "ionic channels" (or the "HBr$^+$ ionic channel" and the "HBr^{+*} ionic channel" when referred to separately). The above assignments are in agreement with the work by Loock and coworkers.[27] We note here that we scanned the laser over a broad range of wavelengths in this excitation region looking for Br$^-$ (negative) ions that would confirm the existence of an ion-pair pathway (path iii in Sec. I), but without success.

The Br and Br* channel KER positions show only a slight increase with J' for the $E(v' = 0)$ state but a clear upwards shift with v' = $m + i$ for the V state. The slight increase with J' in the $E(v' = 0)$ state can be explained by the increase in $E(J'')$ which dominates over a decreasing photon energy $(h\nu)$[9,13,34] (See Eqs. 1 (a) – (b)), whereas the clear shift for the V state is due to the increasing photon energy. We note that the "double" or "split" intense rings observed in some of the images that result in "splitting" of the corresponding KER peaks, for the Br and Br*

channels, for the $V(v' = m + i)$ states in particular, are due to the recoil effect as the hydrogen atoms H* ionize to form $H^+ + e^-$.[45]

Comparing the various peak intensities in the E (Fig. 3(a)) and the V (Fig. 3(b)) states KER distributions, it is evident that the Br and Br* channels dominate the H^+ production in both states over the ionic channels. For the $E(v' = 0)$ resonance state, the strongest H^+ signals are observed in the Br channel and the Br*/Br ratio (Fig. 4(a)) reaches a minimum at $J' = 6$ - 7. For the $V(v' = m + i)$ resonance states, the relative intensities of the various ion signals vary with v'. The Br channel dominates at low $v' = m + i$ ($i = 4,5$) whereas the Br* channel dominates at higher v'. The integrated signal intensities reveal that for the V state the Br channel contribution is smallest for $i = 8$ (not shown).

Whereas the Br and Br* channels produce the majority of H^+, the ionic channels feature a number of HBr^+ vibrational peaks. These peak positions remain virtually unchanged with J' for the $E(v' = 0)$ state, whereas, for the V state they exhibit beat structures with increasing number of peaks as $v' = m + i$ increases. The calculated KER peak positions for the ionic channels (Section I, path (ii) and Eq. 1(c) and (d)) are shown above the respective peaks in Fig. 5. Furthermore, the energies of the maximum vibrational levels observed in each spectra ($E(v^+_{max})$) are found to match closely the sum of the molecular ground state internal energy (rotational energy) and the three-photon excitation energy, i.e.

$$E(v^+_{max}) \approx E(J'') + 3h\nu \tag{4}$$

The intensity fluctuations observed in KERs for the ionic channel are partly due to the effect of changing Franck-Condon overlaps of the wavefunctions involved and partly due to overlapping of different peaks in the two vibrational progressions for the $H^+ + Br(^2P_{3/2}) \leftarrow HBr^+(^2\Pi_{3/2})$ and H^+

+ $Br(^2P_{1/2}) \leftarrow HBr^+(^2\Pi_{1/2})$ transitions. The peak structure gradually fades away as v^+ decreases. The vibrational structures could easily be fitted by sum of Gaussian functions, suggesting that each v^+ peak corresponds to a single or few rotational transition from the resonance excited states (See Fig. 5 (c)). Generally the band-widths were found to be larger for the E Rydberg than for the V ion-pair state.

B. Angular distributions of H$^+$

Significant angular distribution variations of the H$^+$ ions for the E state vs. J' and for the V state vs. v' can already be seen in Fig. 2. As J' increases from $J' = 1$ to $J' = 9$ for the E state, the Br* channel distribution changes gradually from a shape corresponding to a parallel transition towards a perpendicular one. The opposite effect is observed for the Br channel. For the $v' = m + i$ vibrational levels of the V state, the Br* channel exhibits a parallel character for all i's except for $i = 6$. The same is observed for the Br channel with the exception of $i = 5$, $J' = 0 - 4$. The ionic channel angular distribution shapes do not exhibit any significant change as the excitation energy changes both for the E and the V states.

In extracting quantitative information from the angular distributions above, we were faced with a difficult dilemma. In the simple case of a single-photon photolysis, followed by photofragment ionization, the angular distribution ($P(\theta)$) can be expressed[46] as

$$P(\theta) = A(1 + \beta_2 P_2(\cos(\theta)) + \beta_4 P_4(\cos(\theta) + \beta_6 P_6(\cos(\theta)))) \quad (5)$$

where P_2, P_4 and P_6 are the second, fourth and sixth order Legendre polynomials. β_2, β_4 and β_6 are the corresponding anisotropy beta parameters and A is a scaling factor. The three beta parameters can then be related to the transition state symmetry and dynamics including vector correlation phenomena such as alignment and orientation.

Whereas most angular distribution treatments associated with VMI studies are based on such one-step direct process analysis, some work on HCl and HBr has been based on two-step processes, i.e. a one-step resonance excitation followed by a second ionization step.[47,48] Here, HBr absorbs two photons to reach a specific v', J' level of the E or the V resonance states, followed by two photons to produce H^+ via the pathways described in Sections I and III.A. Thus the overall process involves the absorption of four photons. Hence, fitting the angular distributions with a function such as Eq. (5), will result in "effective" beta parameters, which can be only loosely related to the ones the reader is familiar with in single-photon cases. On the other hand, the obvious change in the angular distribution of the Br and Br* channels for the E resonance state, requires some kind of quantification. We finally ended up using a form of Eq. 5 limiting the fit to the β_4 term and we discuss the resulting "effective" beta parameters taking into account the multiphoton nature of the H^+ production processes. Where possible, we attempted a two-step analysis. The beta parameters resulting from both approaches for the Br and Br* channels are plotted in Fig. 6.

The β_2 values for the Br* channel of the E state, follow a decreasing trend starting positive around 0.5 for $J' = 1$, changing sign at $J'= 4$ and reaching -0.6 for $J'= 9$. The opposite trend is observed for the Br channel starting at -0.4 for $J'= 1$, changing sign at $J'= 4$ and ending up at 0.27 for $J' = 9$ (Fig. 6 (a)). The fourth Legendre polynomial coefficient (β_4) was used more in order to improve fits rather than to evaluate vector correlation effects. It has mostly negative values, which fluctuate around zero (ranging from -0.3 to 0) as J' changes from 1 to 9 for both Br* and Br channel (Fig. 6 (b)). The Br and Br* channels for the $V(m + 4)$ state both exhibit a downward trend in β_2 as J' increases, with Br* having more positive values than Br at any given J'.

To evaluate how much the crude beta parameters differ from a more appropriate analysis taking into account the multiphoton nature of the processes involved the data for the angular distributions derived for the resonance excitation to $E(v'= 0, J')$ were analysed according to a more appropriate two-step photoexcitation formalism given by Chichinin et al.[48] corresponding to two-photon excitation to the $E(v'= 0,J')$ states followed by one-photon excitation to superexcited states. The observed angular distribution of the photoproduct, $P(\theta)$, is expressed as

$$P(\theta) = A \, P_f(\theta) \, P_{ph}(\theta) \qquad (6)$$

where $P_f(\theta)$ is the angular distribution of the axes in the resonance intermediate state and $P_{ph}(\theta)$ is the photofragment angular distribution produced by the photolysis of the unpolarised intermediate state. $P_f(\theta)$ and $P_{ph}(\theta)$ are expressed as

$$P_f(\theta) = 1 + \beta_{f,2} P_2(\cos(\theta)) + \beta_{f,4} P_4(\cos(\theta)) \qquad (7a)$$

$$P_{ph}(\theta) = 1 + \beta_{ph,2} P_2(\cos(\theta)) + \beta_{ph,4} P_4(\cos(\theta)) \qquad (7b)$$

Expression (6) was used to fit the angular distributions for A, $\beta_{f,4}$, $\beta_{ph,2}$ and $\beta_{ph,4}$ as variables and for $\beta_{f,2}$ estimated from

$$\beta_{f,2} = \frac{2 - 20\,\mathrm{Re}[b]}{2 + 25|b|^2}; \qquad (8)$$

where $\mathrm{Re}[b]$ represents the real part of the parameter b which can be derived from intensity ratios of Q over S (i.e. I_Q/I_S) and Q over O (I_Q/I_O) rotational lines from

$$\frac{I_Q}{I_S} = \frac{10}{3}\frac{(2J''+1)}{(J''+2)}\left[|b|^2\frac{(2J''+3)}{(J''+1)} + \frac{1}{5}\frac{J''}{(2J''-1)}\right]$$
$$\frac{I_Q}{I_O} = \frac{10}{3}\frac{(2J''+1)}{(J''-1)}\left[|b|^2\frac{(2J''-1)}{J''} + \frac{1}{5}\frac{(J''+1)}{(2J''+3)}\right] \qquad (9)$$

where J'' is the rotational quantum number for the ground state. Furthermore, the alignment parameter, A_{20}, for $J'= 1$ can be derived from
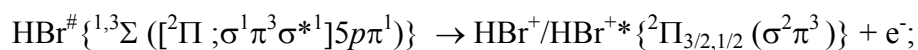
$$A_{20} = \frac{10\,\text{Re}[b]-1}{25|b|^2+2} \tag{10}$$

Based on line intensity ratios evaluated from mass resolved $(2 + n)$ REMPI spectra of

HBr, for the $E(v'= 0)$ state, $b^2 = 1.2$ ($b = 1.1$) was obtained by Eq. (9). This gave $A_{20} = +0.31$ for

$J'= 1$ by Eq. (10) and $\beta_{f,2}= -0.62$ by Eq. (8). The A_{20} value (+0.31) can be compared with the

extreme values of $A_{20}{}^{\text{max}} = + 0.5$ and $A_{20}{}^{\text{min}} = - 1$ for dominating perpendicular and parallel

transitions respectively[48,49] and the β_{f2} value (-0.62) can be compared with the corresponding

extreme values of -1 (perpendicular) and +2 (parallel). The results are plotted in Figs. 6(a) and

6(b). The $\beta_{ph,2}$ parameters for both Br and Br* exhibit similar trends as in the one-step analysis,

however, their values are all positive, ranging from 0 to ~1.4 (Fig. 6(c)). The $\beta_{ph,4}$ parameters

fluctuate around 0 (Fig. 6(d)) .

IV.   DISCUSSION

The trend seen in Fig. 4(a), for the Br*/Br ratio is similar to what has been found in REMPI

work[35] for the total ion signal intensities of Br^+ ($I(Br^+)$) over that for the total ion signal

intensities of HBr^+ ($I(HBr^+)$) (i.e. $I(Br^+)/I(HBr^+)$) as well as line-widths of ion signal intensities.

Both, have been explained to be associated with J' dependent state mixing between the $E(v'= 0)$

Rydberg state and the $V(v'= m + 4)$ and $V(m + 5)$ ion-pair states.[35] This similarity suggests that

the relative ion signals for the Br* and Br channels are also indicative of the state mixing. The

state mixing between a Rydberg state and an ion-pair vibrational state depends on the state

interaction strength, which, to a first approximation, is proportional to the vibrational

wavefunction overlap. Furthermore, the mixing, which holds for J' levels of equal values only,

increases as the energy difference between the energy levels decreases (see Fig. 4 (b)). Thus, the

mixing between the $E(v'= 0)$ and the $V(v'= m + 4)$ states decreases as J' increases whereas the

14

mixing between $E(v'= 0)$ and $V(v'= m +5)$ increases with J'. By comparison, therefore, we conclude that enhanced H^+ signals due to the Br* channel (and also the ionic channels (Fig. 4a)) relative to that for the Br channel is an indication of a mixing of the $E(v'= 0)$ and V ($V(v'= m + 4)$ and $V(v'= m + 5)$) states or, in other words, that an increased ion-pair character of the $E(v'= 0)$ state favours the Br* and the ionic channels over the Br channel.

As can be seen in Fig. 1, favourable (Franck-Condon wise) transitions to the Rydberg state(s) which correlate with H* + Br* (Br* channel) might in fact occur close to the outer turning point of the V well, i.e. to the higher energy component of the $^{1,3}\Sigma$ ($[^2\Pi;\sigma^1\pi^3\sigma^{*1}]5p\pi^1$) states. This could explain why the Br* channel is favoured over the Br channel as the ion-pair character increases. Transitions from shorter internuclear distances (hence smaller V state character) to the $^{1,3}\Pi$ ($[B^2\Sigma^+;\sigma^2(\pi_x^1\pi_y^1)\sigma^{*1}]5p\pi^1$) Rydberg state correlating with H* + Br, on the other hand, might play an important role in Br channel (see Fig. 1). Considering the close correlation seen in the behaviour of the H^+ signals for the Br* and ionic channels (Fig. 4(a)), there is a reason to believe that these channels originate from the same intermediate state(s). We, therefore, propose that the <u>major contribution</u> to the stepwise ionization via the ionic channel formations involves excitation to the higher energy component of the $^{1,3}\Sigma$ ($[^2\Pi;\sigma^1\pi^3\sigma^{*1}]5p\pi^1$) state by excitation (a) in Section I ((b) to a lesser extent) followed by autoionization according to the Auger effect, where the Rydberg electron is removed and the σ^* electron transfers back to the σ orbital to form HBr^+ and $HBr^+*/$ $^2\Pi_{3/2,1/2}$ ($\sigma^2\pi^3$), i.e.

$$HBr^\#\{^{1,3}\Sigma\ ([^2\Pi;\sigma^1\pi^3\sigma^{*1}]5p\pi^1)\} \rightarrow HBr^+/HBr^+*\{^2\Pi_{3/2,1/2}\ (\sigma^2\pi^3)\} + e^-;$$

Autoionization

As mentioned in the results section, the $\beta_{f,2}$ value (-0.62) can be compared with the corresponding extreme value of -1 for a perpendicular transition. This suggests that the resonance transition corresponds to a dominating perpendicular two-photon transition (i.e. $\Sigma \leftarrow \Pi \leftarrow \Sigma$).[48] This is in agreement with earlier observations by Loock and coworkers who came to the conclusion that the transition involved about 20% contribution of the parallel excitation pathway ($\Sigma \leftarrow \Sigma \leftarrow \Sigma$).[27] Comparison of the β_2 and $\beta_{ph,2}$ values of Fig. 6 shows the effect of performing a two-step excitation analysis rather than an analysis based on a one-step excitation process only. Thus, the β_2's, for the overall process, (Fig.6(a)) for the signals derived for the Br* and Br channels cross the border value of zero which separates mostly parallel transitions ($0 < \beta_2 < 2$) from mostly perpendicular ones ($-1 < \beta_2 < 0$) as J' changes, whereas the $\beta_{ph,2}$'s, for the second excitation steps are larger than zero in all cases, corresponding to mostly parallel transitions for all J's. Clearly the contribution of a perpendicular transition increases for Br* but decreases for Br in the second excitation step as J' increases, whereas the corresponding transitions via HBr$^+$ and HBr$^+$* are virtually purely parallel in nature, independent of J'.   Judging from this and the arguments above, the parallel transitions (Section I, (a) and (b)) corresponding to the excitations to the $^{1,3}\Sigma$ ($[^2\Pi ;\sigma^1\pi^3\sigma^{*1}]5p\pi^1$) states to form mainly H* + Br* but to a lesser extent H* + Br, are dominant for $J' = 1 - 9$. The J' dependence of the $\beta_{ph,2}$ values, however, suggests that the contribution of the perpendicular transition (Section I, (c)) to $^{1,3}\Pi$ ($[B^2\Sigma^+;\sigma^2(\pi_x{}^1\pi_y{}^1)\sigma^{*1}]5p\pi^1$) to form H* + Br increases with J'. Increasing contribution of a perpendicular transition associated with the formation of H* + Br* as J' increases must be associated with curve crossings.
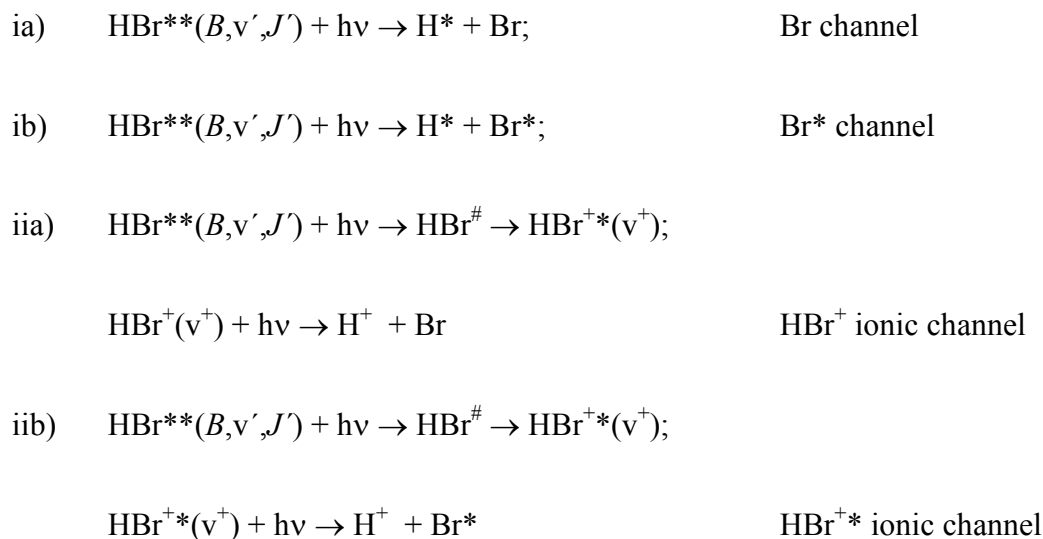
Due to low rotational line intensities for the $V(v' = m + i)$; $i = 4 - 10$ states, hence inaccuracy in the evaluations of intensity ratios I_Q/I_S and I_Q/I_O (Eq. 9), the corresponding angular distributions could not be analysed according to the two-step formalism described above and used

16

for $E(v'=0)$. Instead they were analysed by the single step approximation method (Eq. 5). There is, however, a reason to believe that the first step involves a dominating parallel transition as in the case of the resonance excitation to the $E(v'=0)$ state. Therefore, based on the comparison of the two methods of analysis for the $E(v'=0)$ state, the β_2 parameters derived for the $V(v'=m+i)$ states can be viewed as lower limit values for the corresponding dissociation steps ($\beta_{ph,2}$). β_2 and β_4 values are plotted in Fig. 6 as a function of i for $J'=0$. The plot of the anisotropy parameter, β_2 vs. i (Fig. 6) for the Br channel reveals two minima (enhanced perpendicular transition contributions) for $i=5$ and 9. These correspond to the V vibrational states, which, along with the $i=4$ and 8 states, are closest in energy to the $E(v'=0)$ and $E(v'=1)$ states respectively.[16,17] This could be associated with an enhanced E state character, hence increased contribution of the perpendicular transition to the $^{1,3}\Pi$ ($[B^2\Sigma^+;\sigma^2(\pi_x^1\pi_y^1)\sigma^{*1}]5p\pi^1$) state. The sudden drop in β_2 vs. i observed for $i=6$, (Br* channel), was a bit of a surprise. REMPI spectra of HBr show weak peak structure close to the $V(v'=m+6; J'=0)$ band which must be Q lines of a Rydberg state. Ginter et al.[9] as well as Callaghan and Gordon[13] have assigned spectra in this region to the $f\,^3\Delta_1$ Rydberg state. Most likely, therefore, the "sudden" enhanced perpendicular transition contribution observed is associated with a $V(v'=m+6)$ to Rydberg state interaction, either directly or via a gateway Rydberg state. Finally, the transitions via HBr$^+$ and HBr$^+$* are found to be virtually purely parallel in nature analogous to that found for $E(v'=0)$.
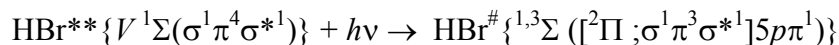
V. CONCLUSIONS

Proton photoion images were recorded following $(2+n)$ REMPI of HBr via the mixed E $(^1\Sigma^+)$ Rydberg and $V(^1\Sigma^+)$ ion-pair states (the mixed $B(^1\Sigma^+)$ state) for $v'=0$ in the E state and $v'=$

$m + i$; i = 4 – 10 in the V state, for a number of rotational levels ($J' = J''$/ Q lines). Kinetic

energy release and angular distributions were derived from the data. Four major dissociation

channels were detected:

ia)   HBr**(B,v',J') + hv $\rightarrow$ H* + Br;   Br channel

ib)   HBr**(B,v',J') + hv $\rightarrow$ H* + Br*;   Br* channel

iia)   HBr**(B,v',J') + hv $\rightarrow$ HBr$^{\#}$ $\rightarrow$ HBr^{+}*(v^{+});

         HBr$^{+}(v^{+})$ + hv $\rightarrow$ H^{+} + Br   HBr^{+} ionic channel

iib)   HBr**(B,v',J') + hv $\rightarrow$ HBr$^{\#}$ $\rightarrow$ HBr^{+}*(v^{+});

         HBr^{+}*(v^{+}) + hv $\rightarrow$ H^{+} + Br*   HBr^{+}* ionic channel

The KER and angular distributions for the different channels vary largely, depending on v' and J'

for excitations to the V and the E states. The KER spectra were assigned and found to agree with

previous work. Br*/Br KER peak ratios in comparison with mass resolved REMPI spectra data

suggest that channel (ia) is largely associated with the E Rydberg state character of the mixed

state whereas the other channels (ia, iia and iib) are to a large extent associated with the V ion-

pair state character. Angular distributions were analyzed to determine anisotropy parameters by a

single as well as a two-step photoexcitation formalism[48] where possible. The analysis revealed a

dominating perpendicular transition for the resonance excitation steps, but mostly parallel

transitions for the dissociation steps with some perpendicular contribution character for the

dissociation steps, varying with J' for the E(v' = 0) state and with v' for the V(v' = $m + i$) states for

channels (ia) and (ib). Our results suggest that the corresponding major   parallel and

perpendicular photoexcitation transitions, following the resonance excitations, involve transitions

18

to singlet or triplet superexcited Rydberg states, which converge to the excited ionic states $B^2\Sigma^+$ and $^2\Pi_{3/2,1/2}$ and which correlate to the neutral fragments $H^*(n = 2) + Br(^2P_{3/2})$ and $H^*(n = 2) + Br^*(^2P_{1/2})$, i.e.
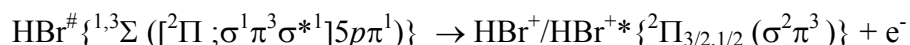
$$HBr^{**}\{V\,^1\Sigma(\sigma^1\pi^4\sigma^{*1})\} + h\nu \rightarrow HBr^\#\{^{1,3}\Sigma\,([^2\Pi\,;\sigma^1\pi^3\sigma^{*1}]5p\pi^1)\}$$

parallel transition (ib,iia,iib)

$$HBr^{**}\{E\,^1\Sigma([^2\Pi;\sigma^2\pi^3]5p\pi^1)\} + h\nu \rightarrow HBr^\#\{^{1,3}\Pi\,([B^2\Sigma^+;\sigma^2(\pi_x^1\pi_y^1)\sigma^{*1}]5p\pi^1)\};$$

perpendicular transition (ia)

The major formation of $HBr^+(3/2,v^+)$ and $HBr^+*(1/2,v^+)$ (iia, iib) then involves autoionization according to the Auger effect,

$$HBr^\#\{^{1,3}\Sigma\,([^2\Pi\,;\sigma^1\pi^3\sigma^{*1}]5p\pi^1)\} \rightarrow HBr^+/HBr^+*\{^2\Pi_{3/2,1/2}\,(\sigma^2\pi^3)\} + e^-$$

ACKNOWLEDGMENTS

Figure captions:

Fig. 1

Potential curves of the states involved in H^+ formation following two-photon excitation of HBr to the E and V states (mixed $B^1\Sigma^+$ state), including asymptotic energies of fragments[42] (right). Potential curves for the ion states (broken curves) are derived from Ref. [38]. The repulsive Rydberg states, $[B^2\Sigma]Ry$ and $[^2\Pi]Ry$ (solid blue curves) which correlate to $H^*(n=2) + Br$ and $H^*(n=2) + Br^*$ are similar in shape to the ion curves, $B^2\Sigma$ and $^2\Pi$, (Ref: [38]) but shifted to the respective asymptotes. The potential curve for the B state was derived from Fig. 1 in Ref.26. The vertical arrow represents a possible transition following a resonance excitation to the $E(v'=0)$ state (see text).

Fig. 2:

H^+ velocity map images for (a) $J'=1$, (b) $J'=4$,(c) $J'=7$, (d) $J'=9$ levels of the E ($v'=0$) and for (e) $v'=m+5$ (f) $v'=m+6$ (g) $v'=m+8$ and (h) $v'=m+10$ levels of the V ($v'=m+i$) states of HBr. The laser polarization is indicated by the double arrow. All the images show two intense rings for low and medium kinetic energy releases and number of weaker rings for higher kinetic energy release.

Fig. 3:

a) H^+ kinetic energy release curves (KER's) for resonance excitation from the ground states X ($v'=0$, J'') to the E ($v'=0$; $J'=1$ - 9) states for $J'=J''$ (Q lines). Br, Br* and ionic channel peaks are marked (see H* + Br*, H* + Br and HBr^+*/HBr^+). The curves are normalized to the height of the Br peak. Predicted KER's for the Br and Br* channels are shown as red bars. Horizontal red broken lines in the region for the ionic channels are to guide the eye.

b) H^+ kinetic energy release curves for resonance excitation from the ground states X (v´= 0, J´´) to the V (v´= m + i; i = 4 – 10) states for $J´=J´´=0$ (Q lines). The curves are normalized to the height of the peaks for the Br (i.e. H*+ Br) channel.

Fig. 4:

a) Ratios of integrated H^+ signal intensities as a function of $J´$: Signals for the Br* channel over signals for the Br channel (see (i) in Section I; open circles, dashed fit curve; left axis) and signals for the ionic (HBr^+/HBr^+*) channels over signals for the Br channel (see (ii) in Section I; filled circles, dotted fit curve; right axis).

b) Rotational energy levels, derived from observed REMPI rotational peaks for the E (v´= 0) and the V (v´= m + i); i = 4, 5 states. Level-to-level off-resonance interactions between the V(v´= m + i) ion-pair states and the E(v´= 0) Rydberg state are indicated by broken and unbroken lines.

Fig. 5:

Assignment and analysis of H^+ kinetic energy release curves for the ionic (HBr^+* and HBr^+) channels (see (ii) in Section I) for resonance excitation from the ground states X (v´= 0, J´´) to V (v´= m + i; i = 4,5,6), $J´=J´´=$ 0 (a), to V (v´= m + i; i = 7,8,10), $J´=J´´=$ 0 (b) and to E (v´= 0) $J´=J´´=$ 1 (c). Predicted peak positions / peak assignments due to v^+ excitations are shown above spectra (a-c). Gaussian multi-peak fit of the spectral structure for the resonance excited state E (v´= 0) $J´$ = 1 is shown in (c). Arrows in Fig. (c) indicate peaks which are dominantly due to HBr^+ (v^+ = 12; right) and HBr^+* (v^+ = 10; left) formation.

Fig. 6:

Anisotropy parameters extracted for the $E(v´= 0)$ and $V(v´= m + i)$ states. Top: β_2 (a) and β_4 (b) derived by "single step analysis" (see text) for the H*+Br (blue) and H*+Br* (red) channels of the $E(v´= 0)$ state vs $J´$. Middle: $\beta_{phi,2}$ (c) and $\beta_{phi,4}$ (d) derived by " two-step analysis" (see text) for the H*+Br (blue) and H*+Br* (red) channels of the $E(v´= 0)$ state vs $J´$, Bottom: β_2 (e) and β_4 (f) derived by "single step analysis" for the H*+Br (blue) and H*+Br* (red) channels of the $V(m + i)$ state vs i.

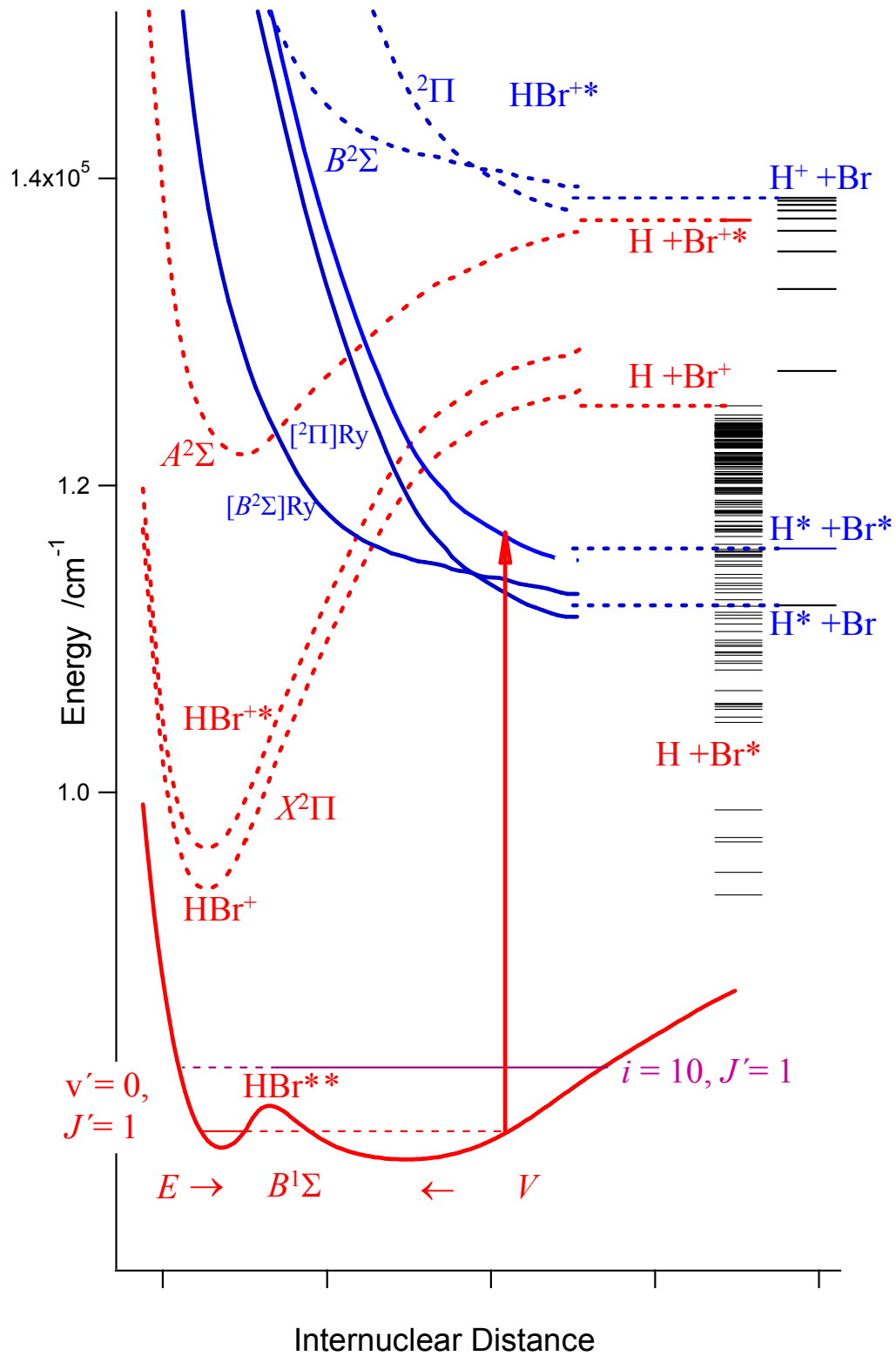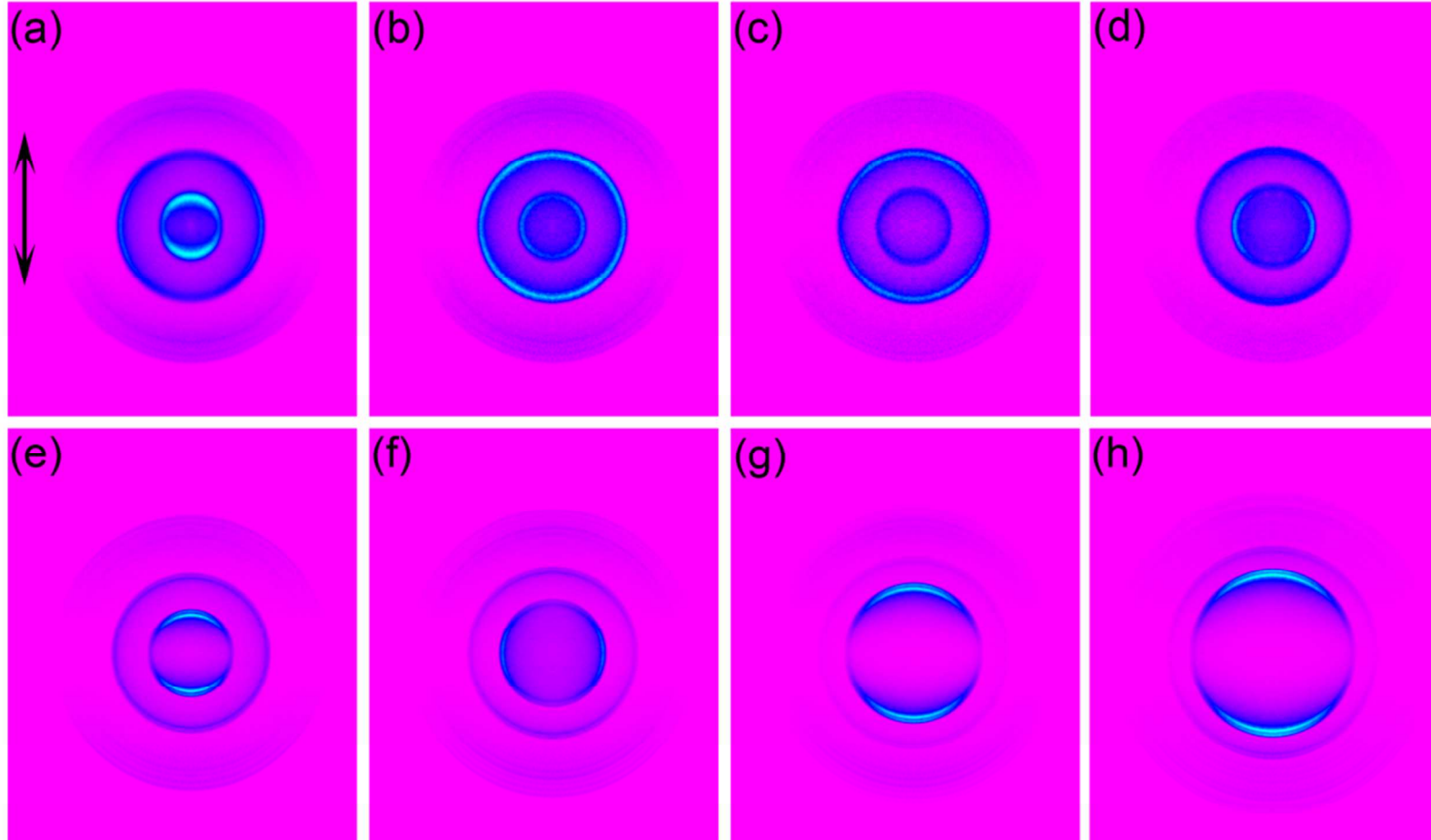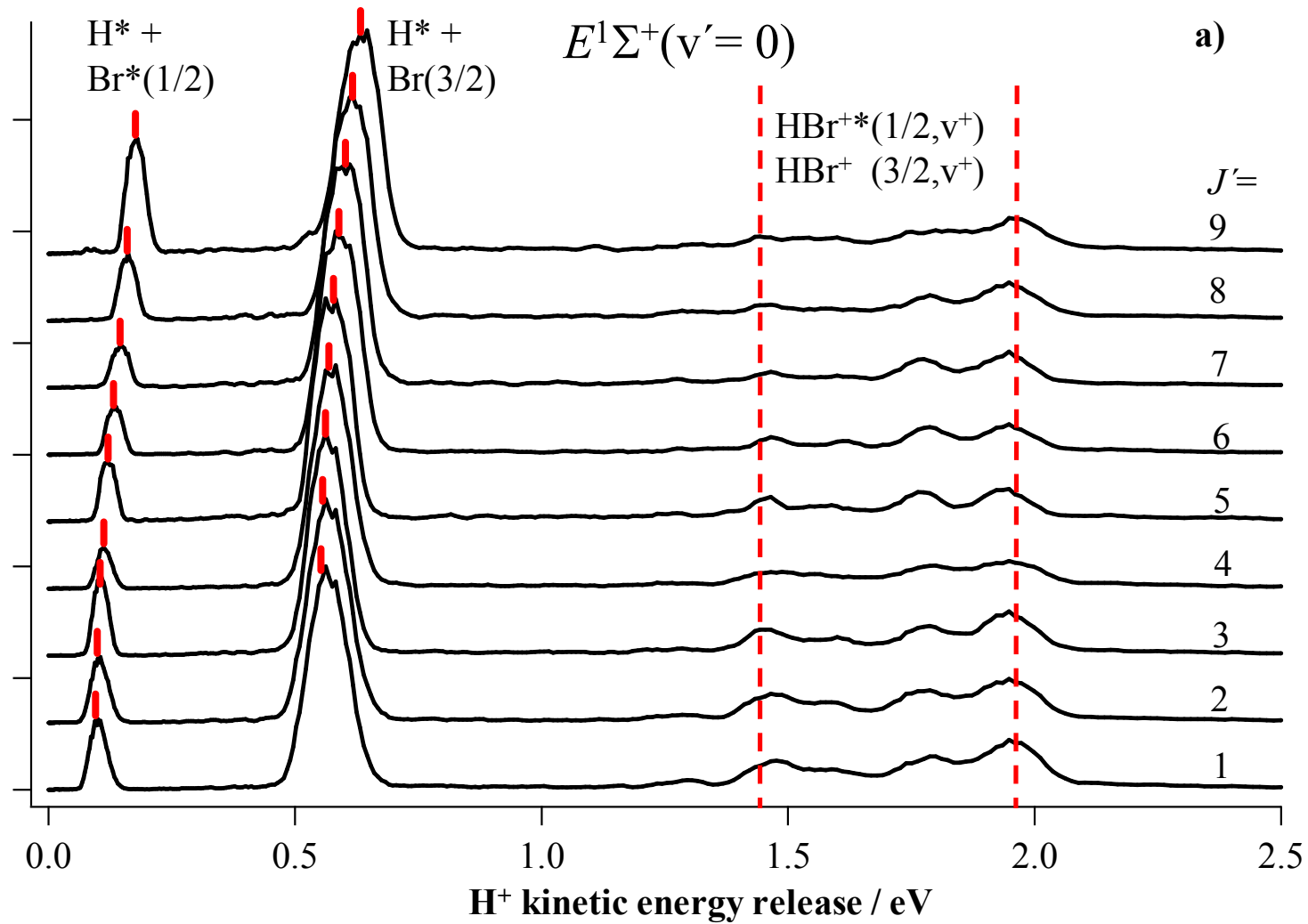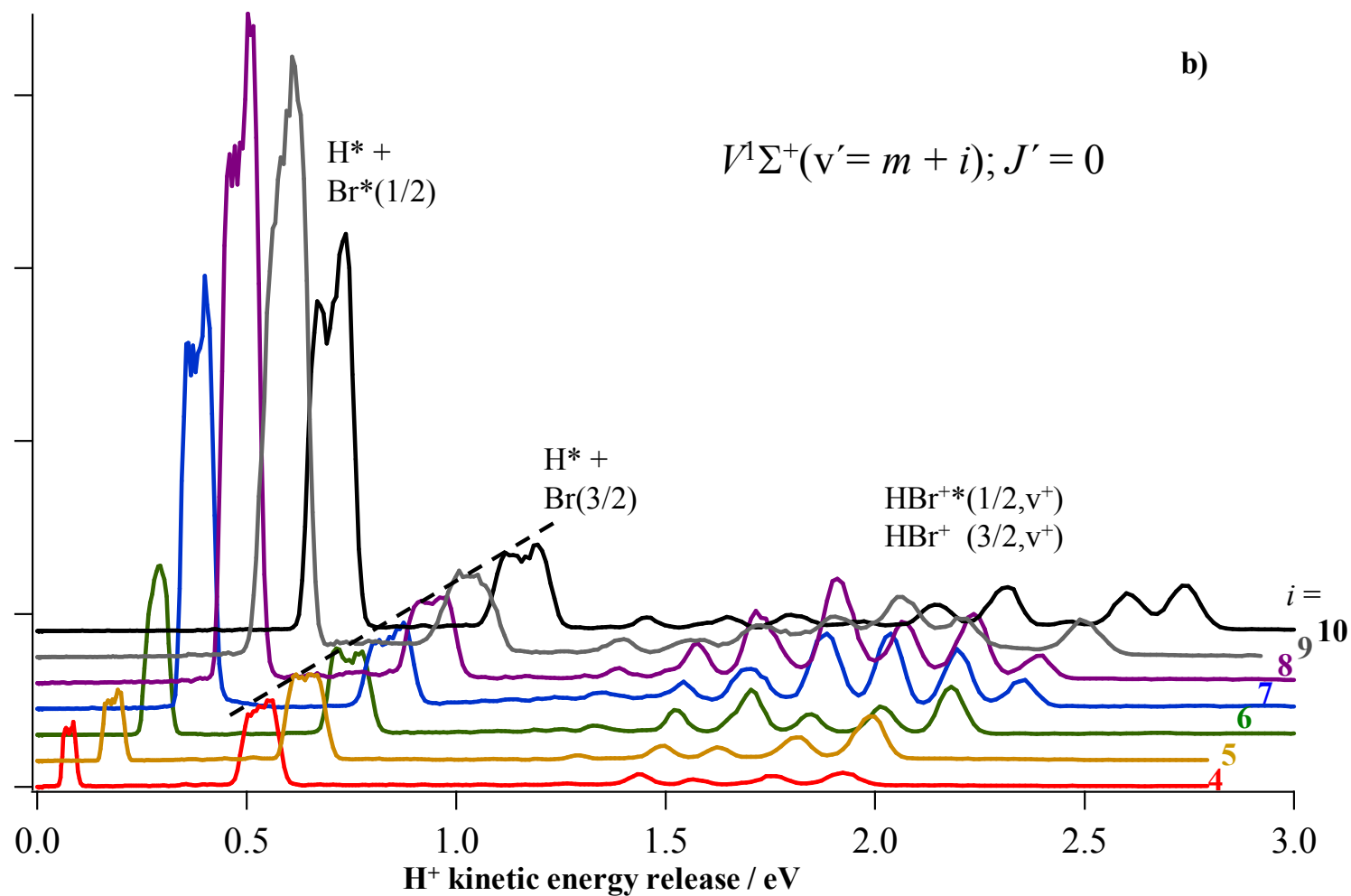**Fig. 1**

Fig. 2

H* + Br*(1/2)

H* + Br(3/2)

$E^1\Sigma^+(v'=0)$

a)

HBr$^+$*(1/2,v$^+$)
HBr$^+$ (3/2,v$^+$)

$J'=$
9
8
7
6
5
4
3
2
1

0.0   0.5   1.0   1.5   2.0   2.5

H$^+$ kinetic energy release / eV

Fig. 3 a

b)

$$V^1\Sigma^+(v'= m + i); J' = 0$$

H* +
Br*(1/2)

H* +
Br(3/2)

HBr$^+$*(1/2,v$^+$)
HBr$^+$ (3/2,v$^+$)

$i =$

10

9

8

7

6

5

4

H$^+$ kinetic energy release / eV

0.0   0.5   1.0   1.5   2.0   2.5   3.0
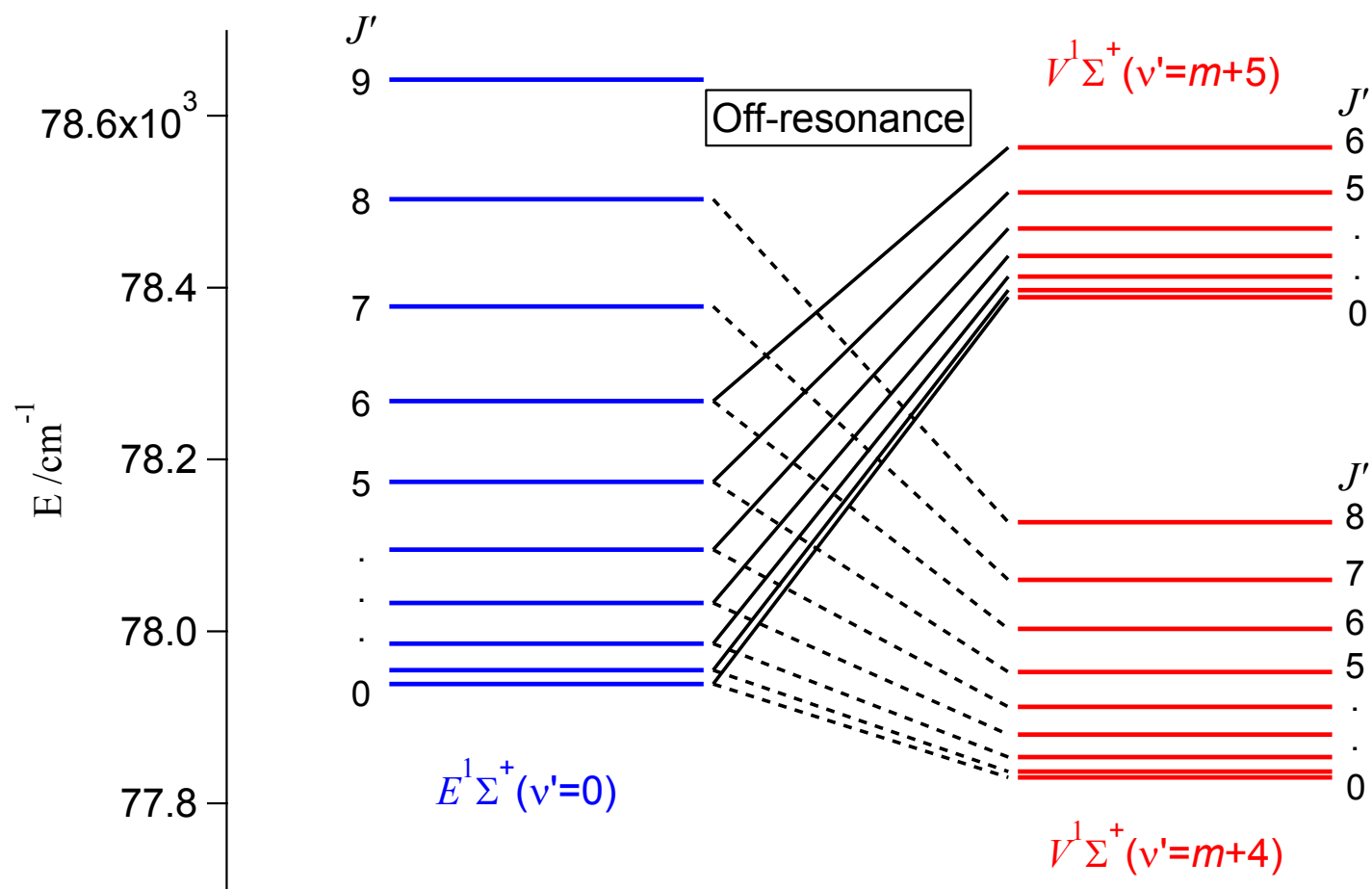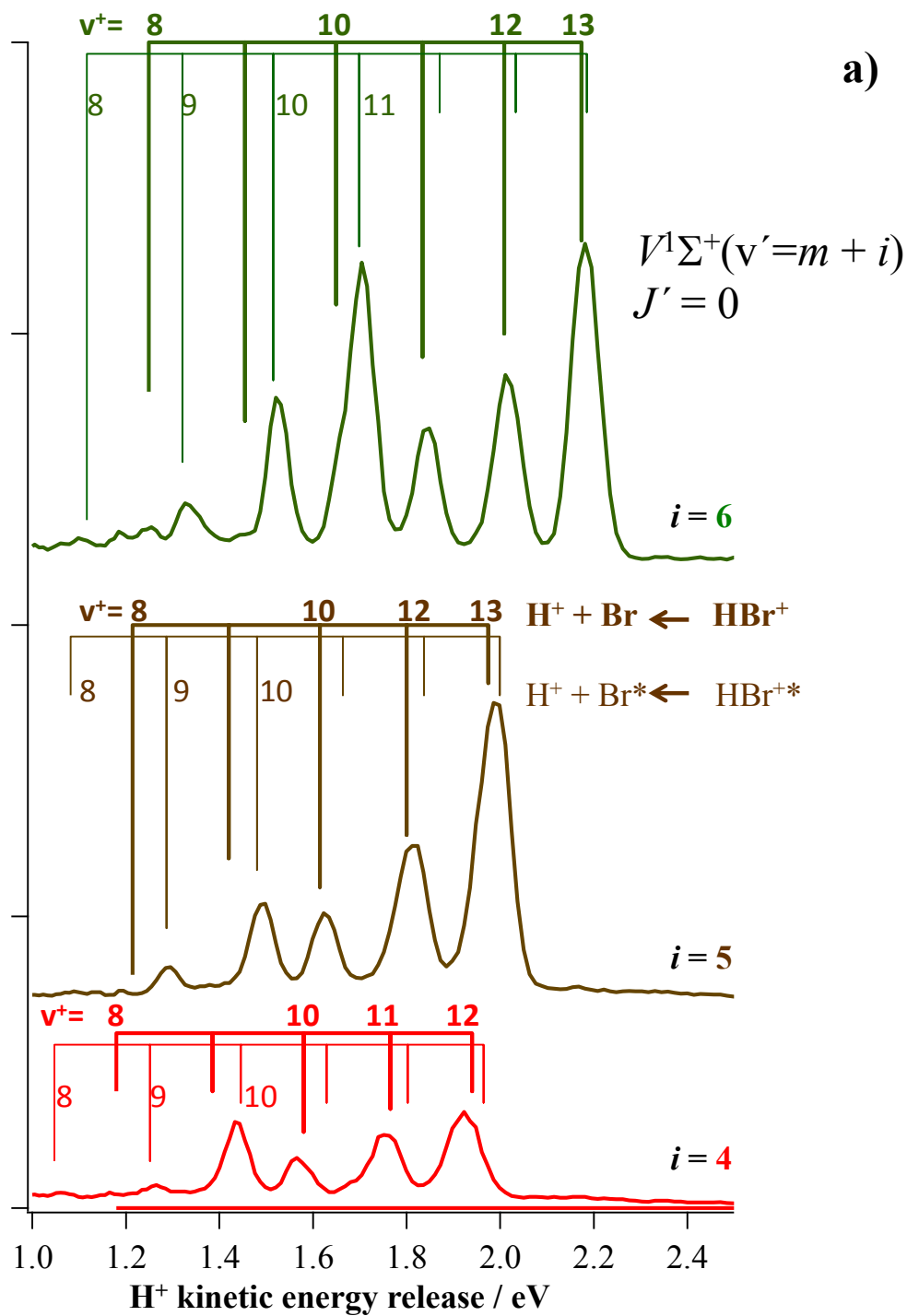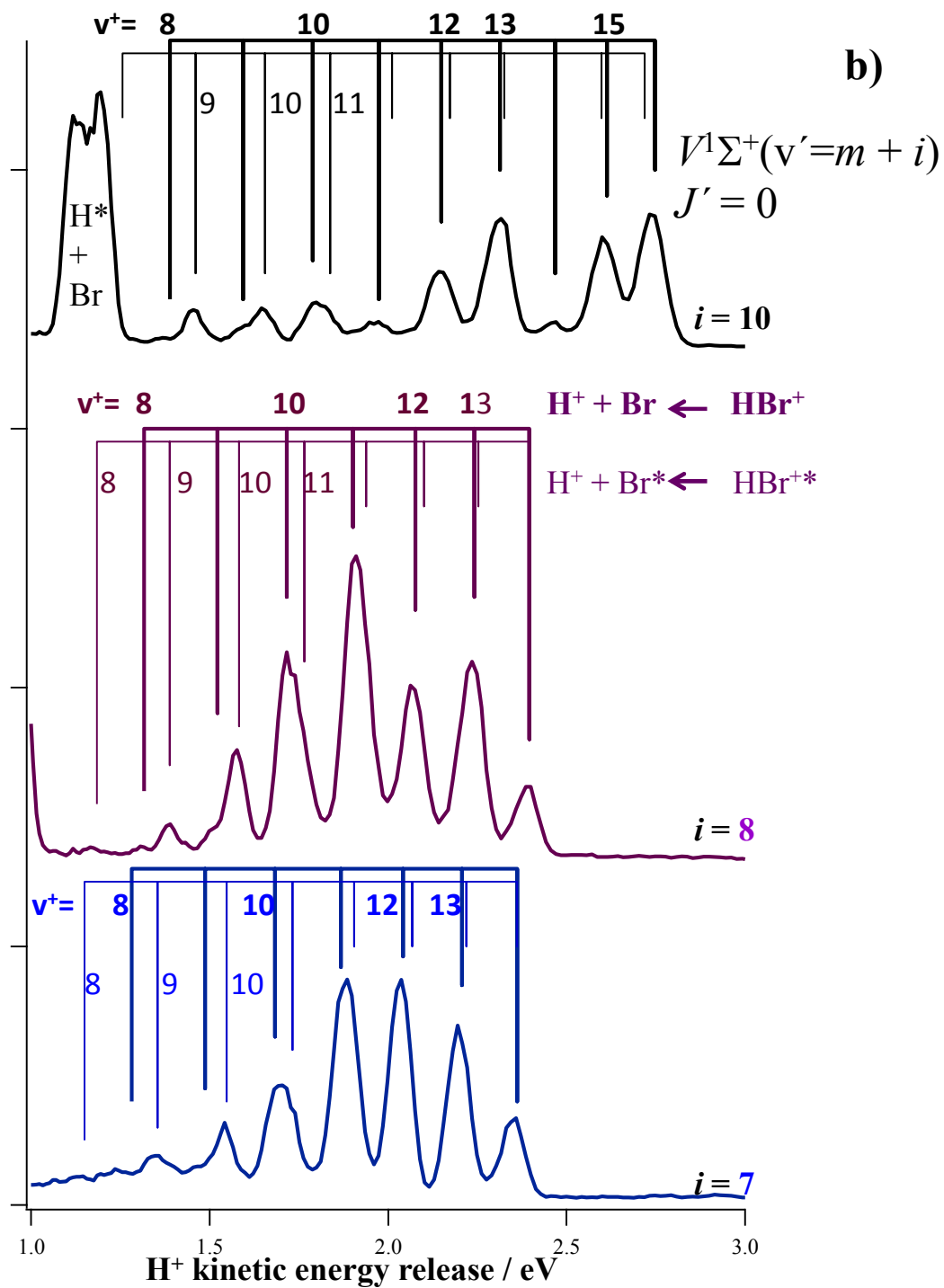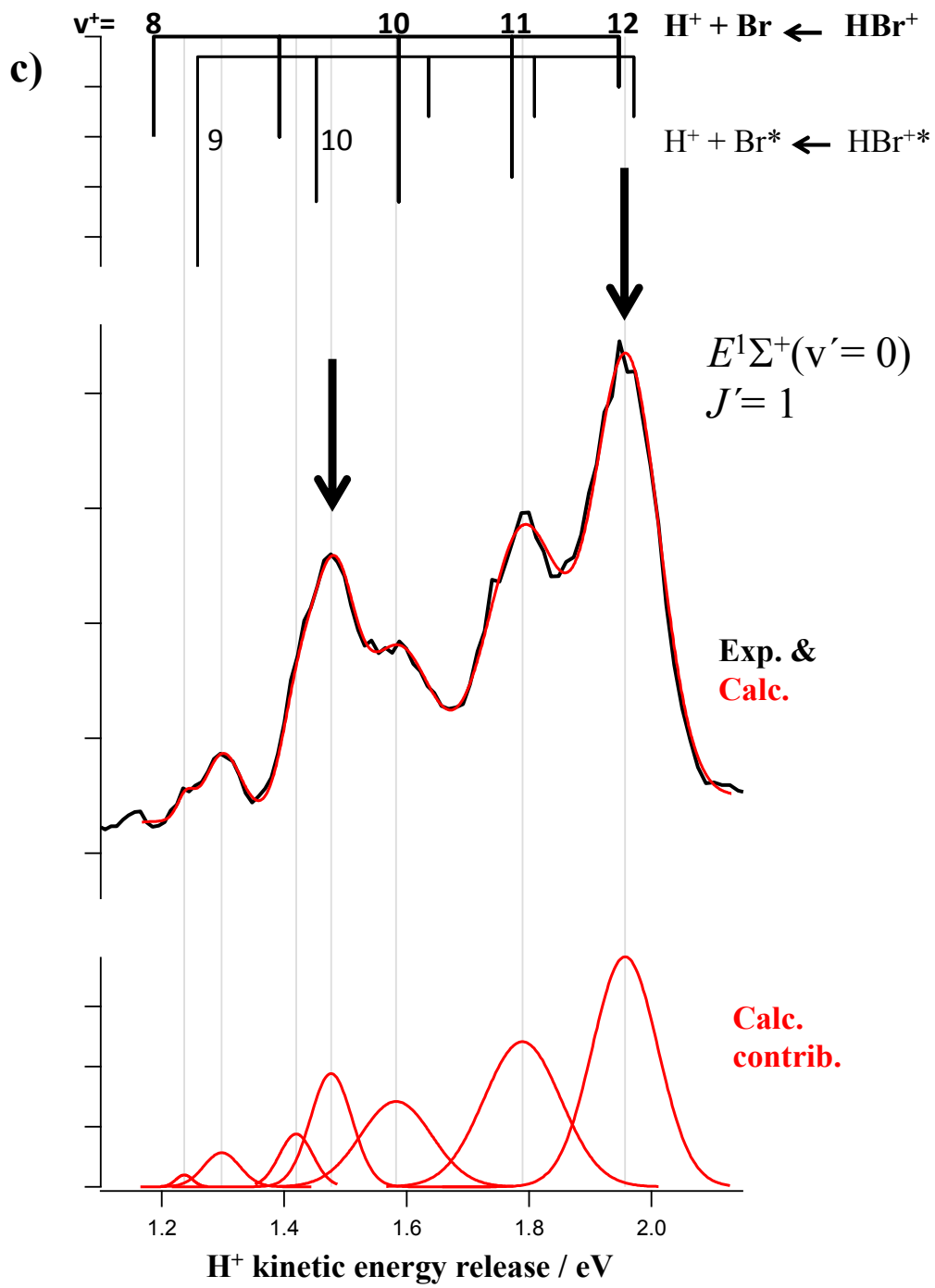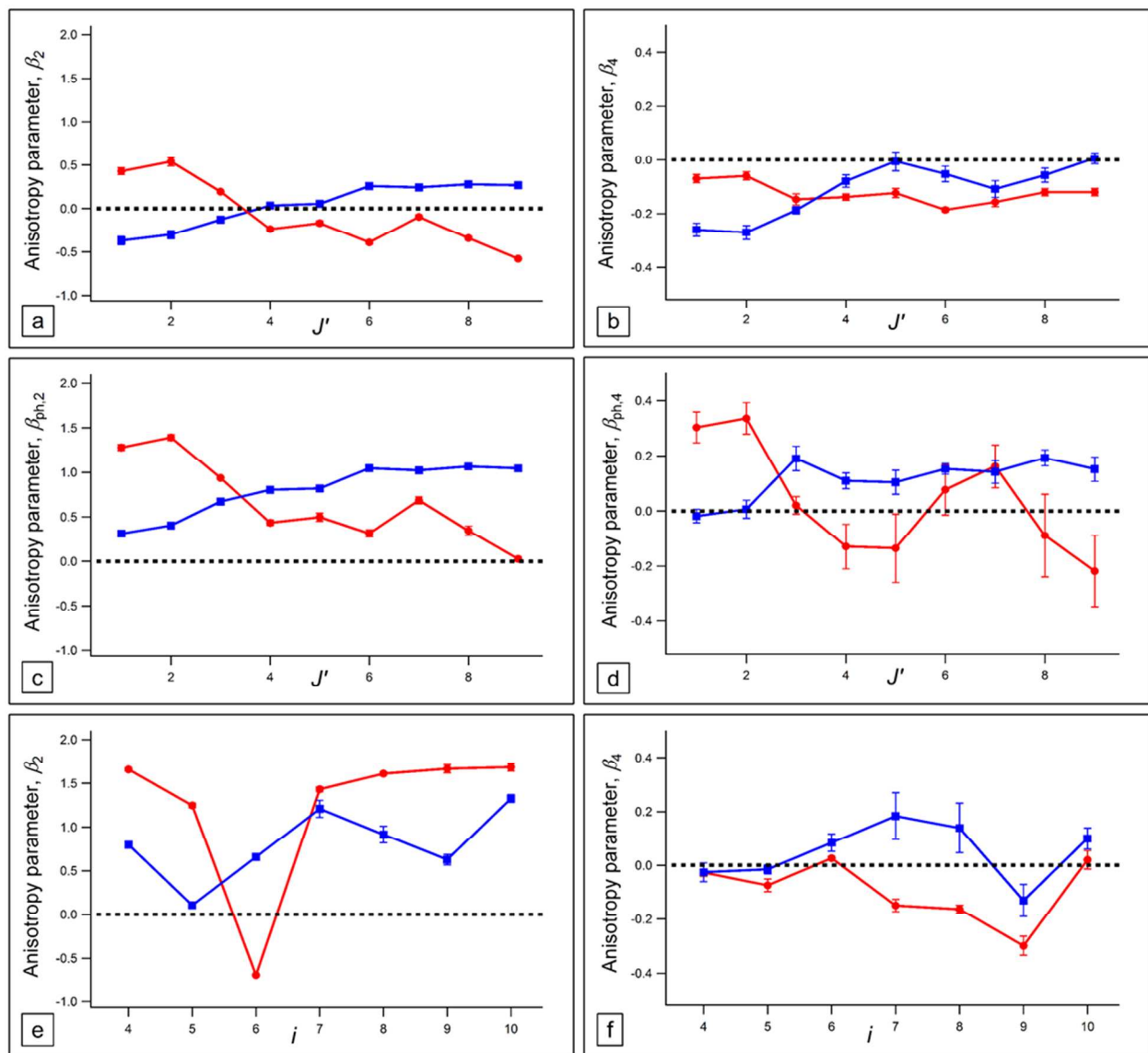
Figs 3 b
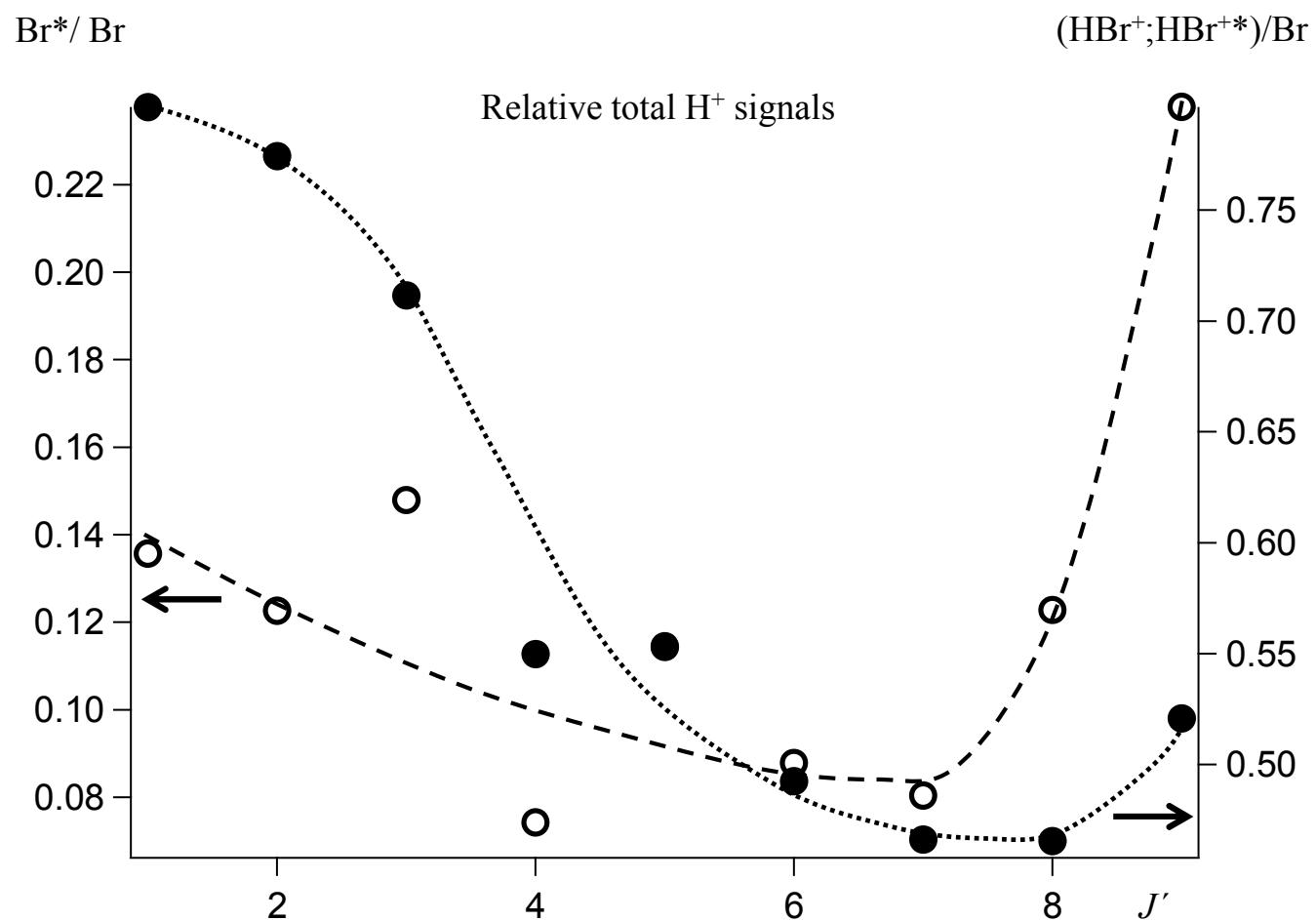
Fig. 4 a

Fig. 4 b

Fig. 5 a

Fig. 5 b

Figs. 5 c

Figs. 6 (a) – (f)

Table I. HBr resonance excited states (Term symbols, vibrational quantum numbers (v´) and rotational quantum numbers (J´)) and two-photon excitation wavenumber (v). NB: m is an unknown integer number.

State	v´	J´	Q lines; ν / cm^{-1}	Refs. / Comment
$E^1\Sigma^+$	0	1	77 938.8	13
		2	77 935.6	13
		3	77 931.6	13
		4	77 926.5	13
		5	77 920.6	13
		6	77 913.5	13
		7	77 905.4	13
		8	77 895.6	13
		9	77 883.0	13
$V^1\Sigma^+$	m +4	0	77 830.0	This work
		1	77 821.0	This work
		2	77 803.0	This work
		3	77 778.7	Derived from Ref. 9
		4	77 743.6	Derived from Ref. 9
		5	77 700.1	Derived from Ref. 9
		6	77 648.2	Derived from Ref. 9
		7	77 587.9	Derived from Ref. 9
		8	77 520.0	Derived from Ref. 9
$V^1\Sigma^+$	m +5	0	78 388.8	13
		1	78 380.2	13
		2	78 362.4	13
		3	78 338.6	13
		4	78 300.6	This work
$V^1\Sigma^+$	m+6	0	78 940.2	13
$V^1\Sigma^+$	m+7	0	79 480.3	13
$V^1\Sigma^+$	m+8	0	80 029.7	13
$V^1\Sigma^+$	m+9	0	80 638.0	This work
$V^1\Sigma^+$	m+10	0	81 197.2	13

References:

(1)   Price, W. C. *Proc. Roy. Soc. Ser. A* **1938**, *167*, 216.

(2)   Tilford, S. G.; Ginter, M. L.; Vanderslice, J. T. *J. Mol. Spectrosc.* **1970**, *33*, 505.

(3)   Ginter, M. L.; Tilford, S. G. *J. Mol. Spectrosc.* **1970**, *34*, 206.

(4)   Tilford, S. G.; Ginter, M. L.; Bass, A. M. *J. Mol. Spectrosc.* **1970**, *34*, 327.

(5)   Tilford, S. G.; Ginter, M. L. *J. Mol. Spectrosc.* **1971**, *40*, 568.

(6)   Nee, J. B.; Suto, M.; Lee, L. C. *J. Chem. Phys.* **1986**, *85*, 719.

(7)   Nee, J. B.; Suto, M.; Lee, L. C. *J. Chem. Phys.* **1986**, *85*, 4919.

(8)   Ginter, D. S.; Ginter, M. L. *J. Mol. Spectrosc.* **1981**, *90*, 177.

(9)   Ginter, D. S.; Ginter, M. L.; Tilford, S. G. *J. Mol. Spectrosc.* **1981**, *90*, 152.

(10)   Green, D. S.; Bickel, G. A.; Wallace, S. C. *J. Mol. Spectrosc.* **1991**, *150*, 303.

(11)   Green, D. S.; Bickel, G. A.; Wallace, S. C. *J. Mol. Spectrosc.* **1991**, *150*, 354.

(12)   Green, D. S.; Bickel, G. A.; Wallace, S. C. *J. Mol. Spectrosc.* **1991**, *150*, 388.

(13)   Callaghan, R.; Gordon, R. J. *J. Chem. Phys.* **1990**, *93*, 4624.

(14)   Pratt, S. T.; Ginter, M. L. *J. Chem. Phys.* **1995**, *102*, 1882.

(15)   Wright, S. A.; McDonald, J. D. *J.Chem.Phys.* **1994**, *101*, 238.

(16)   Kvaran, Á.; Logadóttir, Á.; Wang, H. *J. Chem. Phys.* **1998**, *109*, 5856.

(17)   Kvaran, Á.; Wang, H.; Logadóttir, Á. *J. Chem. Phys.* **2000**, *112*, 10811.

(18)   Kvaran, Á.; Waage, B. G.; Wang, H. *J. Chem. Phys.* **2000**, *113*, 1755.

(19)   Kvaran, Á.; Wang, H.; Waage, B. G. *Can. J. Physics* **2001**, *79*, 197.

(20)   Kvaran, Á.; Wang, H. *Molec. Phys.* **2002**, *100*, 3513.

(21)   Kvaran, Á.; Wang, H. *J. Mol. Spectrosc.* **2004**, *228*, 143.

(22)   Matthiasson, K.; Wang, H. S.; Kvaran, A. *J Mol Spectrosc* **2009**, *255*, 1.

(23)   Long, J.; Wang, H.; Kvaran, A. *J. Molecular Spectroscopy* **2012**, *282*, 20.

(24)   Hrodmarsson, H. R.; Wang, H. S.; Kvaran, A. *J Mol Spectrosc* **2013**, *290*, 5.

(25)   Romanescu, C.; Manzhos, S.; Boldovsky, D.; Clarke, J.; Loock, H. *J. Chem. Phys*
2004, *120*, 767.

(26)   Romanescu, C.; Loock, H. P. *Phys. Chem. Chem. Phys.* **2006**, *8*, 2940.

(27)   Romanescu, C.; Loock, H. P. *J. Chem. Phys.* **2007**, *127*, 124304.

(28)   Chichinin, A. I.; Maul, C.; Gericke, K. H. *J. Chem. Phys.* **2006**, *124*, 224324.

(29)   Kauczok, S.; Maul, C.; Chichinin, A. I.; Gericke, K. H. *Journal of Chemical Physics* **2010**, *133*, 24301.

(30)   Maul, C.; Chichinin, A. I.; Gericke, K.-H. *Journal of Atomic, Molecular, and Optical Physics* **2011**, *2011*, 410108.

(31)   Kvaran, Á.; Matthíasson, K.; Wang, H.; Bodi, A.; Jonsson, E. *J. Chem. Phys.* **2008**, *129*, 164313.

(32)   Kvaran, A.; Matthiasson, K.; Wang, H. *J. Chem. Phys* **2009**, *131*, 044324.

(33)   Matthiasson, K.; Long, J.; Wang, H.; Kvaran, A. *Journal of Chemical Physics* **2011**, *134*, 164302.

(34)   Long, J.; Hrodmarsson, H. R.; H.Wang; Kvaran, A. *J. Chem. Phys* **2012**, *136*, 214315.

(35)   Long, j.; Wang, H.; Kvaran, A. *J. Chem. Phys.* **2013**, *138*, 044308.

(36)   Hróðmarsson, H. R.; Wang, H.; Kvaran, Á. *Journal of Chemical Physics* **2014**, *140*, 244304.

(37)   Poretskiy, M.; Chichinin, A. I.; Maul, C.; K.-H.Gericke *Physical Chemistry Chemical Physics; 10.1039/C4CP02244K* **2014**.

(38)   Banichevich, A.; Klotz, R.; Peyerimhoff, S. D. *Mol. Phys.* **1992**, *75*, 173.

(39)   Gebhardt, C. R.; Rakitzis, T. P.; Samartzis, P. C.; Ladopoulos, V.; Kitsopoulos, T. N. *Rev. Sci. Instrum.* **2001**, *72*, 3848.

(40)   Papadakis, V.; Kitsopoulos, T. N. *Rev. Sci. Instrum.* **2006**, *77*, 5.

(41)   Regan, P. M.; Langford, S. R.; Orr-Ewing, A. J.; Ashfold, M. N. R. *J. Chem. Phys.* **1999**, *110*, 281.

(42)   NIST (National Institute of Standards and Technology).

(43)   Yencha, A. J.; Cormack, A. J.; Donovan, R. J.; Lawley, K. P.; Hopkirk, A.; King, G. C. *Chem. Phys.* **1998**, *238*, 133.

(44)   *NIST Chemistry WebBook*; NIST (National Institute of Standards and Technology) Chemistry WebBook.

(45)   Aguirre, F.; Pratt, S. T. *J. Chem. Phys.* **2004**, *121*, 9855.

(46)   Rakitzis, T. P. *Chemical Physics Letters* **2001**, *342*, 121.

(47)   Manzhos, S.; Romanescu, C.; Loock, H. P.; Underwood, J. G. *Journal of Chemical Physics* **2004**, *121*, 11802.

(48)   Chichinin, A. I.; Shternin, P. S.; Godecke, N.; Kauczok, S.; Maul, C.; Vasyutinskii, O. S.; Gericke, K. H. *J. Chem. Phys.* **2006**, *125*, 034310.

(49)   Zare, R. N. *Angular momentum: Understanding spatial aspects in chemistry and physics*; Wiley, 1988.